Journal of Dynamics, Monitoring and Diagnostics, 2026, 5, 199-207
https://doi.org/10.37965/jdmd.2026.1382

ISTP
RESEARCH ARTICLE

Fault Feature Enhancement and Diagnosis Method for UAV Rotor Bearings Based on Amplitude-Modulated Graph Fourier Spectrum

Guangshuai Yang, Meng Li, Daigeng Jiao, Ling Shi, Kun Zhang, and Yonggang Xu
School of Mechanical and Energy Engineering, Beijing University of Technology, Beijing 100124, China

(Received 30 April 2026; Revised 15 June 2026; Accepted 24 June 2026; Published online 24 June 2026)

Abstract: With the increasing integration and diversification of functions in rotating machinery systems, their reliability faces continuous challenges, leading to a corresponding rise in failure rates. Under long-term operating conditions, motor bearings, as key components of the power system, have become one of the most prone to failure due to the large and continuous loads they bear. To address the aforementioned issues, this paper proposes a bearing fault diagnosis method based on an amplitude modulation spectrum model. First, an amplitude modulation framework using the short-time Fourier transform (STFT) is constructed, and the linear kurtosis of the envelope spectrum (LSES) indicator is introduced to quantitatively evaluate fault feature information under different modulation structures. Subsequently, the signal corresponding to the maximum LSES value is selected to construct a graph signal model. Finally, the last K-order spectral components in the graph frequency domain are retained for feature extraction and enhancement. Validation using both simulated signals and experimental signals of bearing inner and outer race faults demonstrates that the proposed method has good feasibility and effectiveness.

Keywords: fault diagnosis; graph signal; rotating bearing; spectral modulation spectrum

I. INTRODUCTION

Rotating machinery is a critical component for power transmission and energy conversion in industrial systems. Its operational stability and reliability directly determine the efficient and safe operation of the entire industrial system [1,2]. Fault detection (FD) and diagnosis serve as essential technical approaches for identifying abnormal operating conditions, reducing downtime, and preventing unexpected failures in this field [3–5]. Bearings are critical components of rotating machinery and are highly susceptible to damage under complex operating conditions. Meanwhile, operating equipment is often accompanied by significant background noise, which poses substantial challenges to traditional time-domain analysis methods. Bearing faults represent the most frequent type of failure in rotating electrical machines, accounting for up to 40% of all faults. This makes bearing FD and diagnosis a key issue in industrial applications and has developed into an important research hotspot, with substantial progress achieved in related methods and technologies. Under strong noise conditions, fault features are often submerged, making fault diagnosis particularly difficult. Therefore, implementing efficient and accurate fault diagnosis has become a crucial prerequisite for ensuring the continuous and reliable operation of equipment [6]. Fault diagnosis technology has attracted extensive research attention and achieved significant progress in engineering applications in recent years [7,8]. Some scholars have conducted extensive research on gear systems and achieved fruitful results. Huangfu Yifan focused on dynamic mechanism modeling and fault tracing of local damage in gear systems. Based on real spalling morphology obtained from fatigue experiments, a gear dynamic model was established and validated to accurately characterize meshing behavior and vibration characteristics [9]. Furthermore, a transmission path analysis method based on in situ testing was proposed, enabling fault localization and feature enhancement from the perspective of the signal transmission mechanism [10].

Bearings are critical components of rotating machinery and are highly susceptible to damage in complex operating environments. Ma *et al.* introduced a dual-objective optimization method relying on reweighted overlapping group sparse shrinkage and frequency slice function (ROGSS-FSF). By integrating harmonic spectral kurtosis (HSK) and Correlation Theil Index (CTI) indicators and employing multi-objective particle swarm optimization (MOPSO) for parameter tuning, the method significantly improves the capability of extracting early-stage bearing fault features under low Signal-to-Noise Ratio (SNR) conditions [11]. To perform difference analysis, Chen *et al.* designed a model that relies on convex optimization, known as the Convex Optimization Difference Analysis (CODA) model. By introducing a dual-spectral-domain differential analysis mechanism and an adaptive weighting strategy, the method enables unsupervised fault diagnosis using only healthy condition data. This approach significantly enhances the capability of extracting fault features in gearboxes and bearings under low SNR conditions [12]. Some scholars have focused their research on frequency domain and time–frequency domain analysis methods. To improve bearing fault feature extraction in complex operating environments, Xu *et al.* presented a convolutional neural network architecture that integrates multi-scale and multi-directional feature aggregation. Experimental validation on multiple bearing datasets demonstrates that the proposed method achieves superior diagnostic performance and robustness

Corresponding author: Kun Zhang (e-mail: zkun212@163.com).

[13]. Jiang *et al.* proposed a spatiotemporal multi-level weighted graph convolutional network to address the fault diagnosis problem of rotating machinery under imbalanced operating conditions. The proposed method significantly improves diagnostic performance and robustness [14]. To enhance the amplitude of fault-induced impulses, Moshrefzadeh proposed a non-linear filtering technique known as spectral amplitude modulation (SAM) [15]. However, the proposed filtering scheme inevitably amplifies noise components as well, which may hinder its performance in real-world applications. Sheng *et al.* introduced EFDSAM, an equalization-filtering approach constructed through differential SAM. By introducing HSK to adaptively determine the optimal differential order and combining it with a frequency-domain averaging segmentation strategy, the method significantly enhances the ability to extract rolling bearing fault features under low SNR conditions [16]. Zhang *et al.* introduced a variable differential spectral amplitude modulation (VDSAM) method and validated its applicability in rolling bearing FD. By introducing the modulation Gini indicator to adaptively determine the optimal differential order and integrating variational filtering with adaptive resonance band identification, the proposed method effectively improves fault feature extraction performance [17].

Spectral graph theory provides the foundation for graph signal processing, an emerging domain that broadens the scope of traditional signal processing to handle information defined on graphs. Xie *et al.* proposed a graph-based multimodal semi-supervised image classification framework (GraMSIC), which significantly improves classification performance for images with imperfect labels by jointly considering label refinement, multi-graph label propagation, and kernel methods [18]. Chuang *et al.* systematically established the theoretical foundation of graph Fourier transform (GFT), where the transform kernel is defined based on the Laplacian and adjacency matrices of graphs, enabling graph signals to be translated from the vertex domain into the graph frequency domain [19]. This theoretical development provides a solid basis for modeling complex systems as graphs and performing fault diagnosis, thereby opening up a new research direction. Sandryhaila *et al.* further utilized the graph adjacency matrix to directly extend classical discrete signal processing methods to the graph domain [20].

To address this issue, this paper proposes an amplitude modulation spectrum model for bearing fault diagnosis. Based on the short-time Fourier transform (STFT), an amplitude modulation spectrum editing method is developed. In addition, a linear kurtosis of the envelope spectrum (LSES) index, which is sensitive to periodic impulsive features, is introduced to quantitatively evaluate the fault information during the spectrum editing process. By constructing a graph signal model based on a modified spectrum, the spectral order can be further selected to reduce noise in the signal and increase diagnostic accuracy.

II. AMPLITUDE MODULATION GRAPH FOURIER SPECTRUM MODEL

In strong noise environments, enhancing the effective information in the signal while suppressing noise is crucial for fault diagnosis of UAV rotor bearings. In this section, an amplitude modulation spectrum editing process is designed to enhance the fault-related features in the signal, and a graph spectrum model is constructed to denoise the edited signal. The overall workflow is illustrated in Fig. 1, and the detailed steps are as follows:

a) An STFT is performed on the time-domain signal to obtain the amplitude and phase details from the original signal.
b) The modulation order (MO) is designed to perform exponential correction of the amplitude, and the fault information in each corrected signal is quantified by the LSES indicator.
c) The corrected signal corresponding to the optimal LSES indicator is selected, and the spectrum of the corrected signal is used for the construction of the graph signal.
d) The graph signal is expanded on the eigenvectors to obtain the spectrum by performing a frequency-domain GFT.
e) The last K orders of the graph are selected for inverse Fourier transform to extract features and achieve fault diagnosis.

a) Amplitude modulation is based on the LSES

SAM was first proposed by Moshrefzadeh *et al.* to apply a MO to the frequency components of the entire signal. However, although SAM enhances fault-related features, it inevitably amplifies certain noise components as well. Within a specific MO range, the amplitude of noise components may even exceed that of the characteristic frequencies, which further complicates bearing fault feature extraction. To overcome this limitation, an STFT-based amplitude modulation method is introduced, which re-expresses the original one-dimensional time-domain signal as a two-dimensional time–frequency distribution. This representation makes it possible to simultaneously characterize signal information in the time and frequency domains, thereby facilitating a more comprehensive analysis and more effective extraction of key fault features. Its definition is given as follows:

$$\begin{aligned} G(t,\omega) &= \int_{-\infty}^{+\infty} x(\tau) g^*(\tau - t) e^{-j\omega\tau} d\tau \\ &= A(t,\omega) e^{j\phi(t,\omega)} \end{aligned} \tag{1}$$

where $x(\tau)$ is the original signal and $g(\tau - t)$ represents the window function. Then, different MO values are assigned to the amplitude information in the time–frequency matrix. Subsequently, this is combined with the original phase, and the inverse STFT is applied; by integrating over time and frequency, a series of corrected signals are obtained, represented as:

$$\begin{aligned} x_m(\tau, MO) = \int_{-\infty}^{\infty} \int_{-\infty}^{\infty} A(t,\omega)^{MO} \\ \times g(t - \tau) e^{j(\omega t + \phi(t,\omega))} dt d\omega \end{aligned} \tag{2}$$

where $x_m(\tau, MO)$ is the correction signal obtained by the proposed method. The range of MO is set between $[-0.5]$ and $[1.5]$, and the information in the correction signal corresponding to each MO is different. If only the square envelope spectrum corresponding to a single (MO) value is selected for analysis, it is still necessary to rely on manual judgment of the energy distribution of each harmonic order. This not only makes the analysis

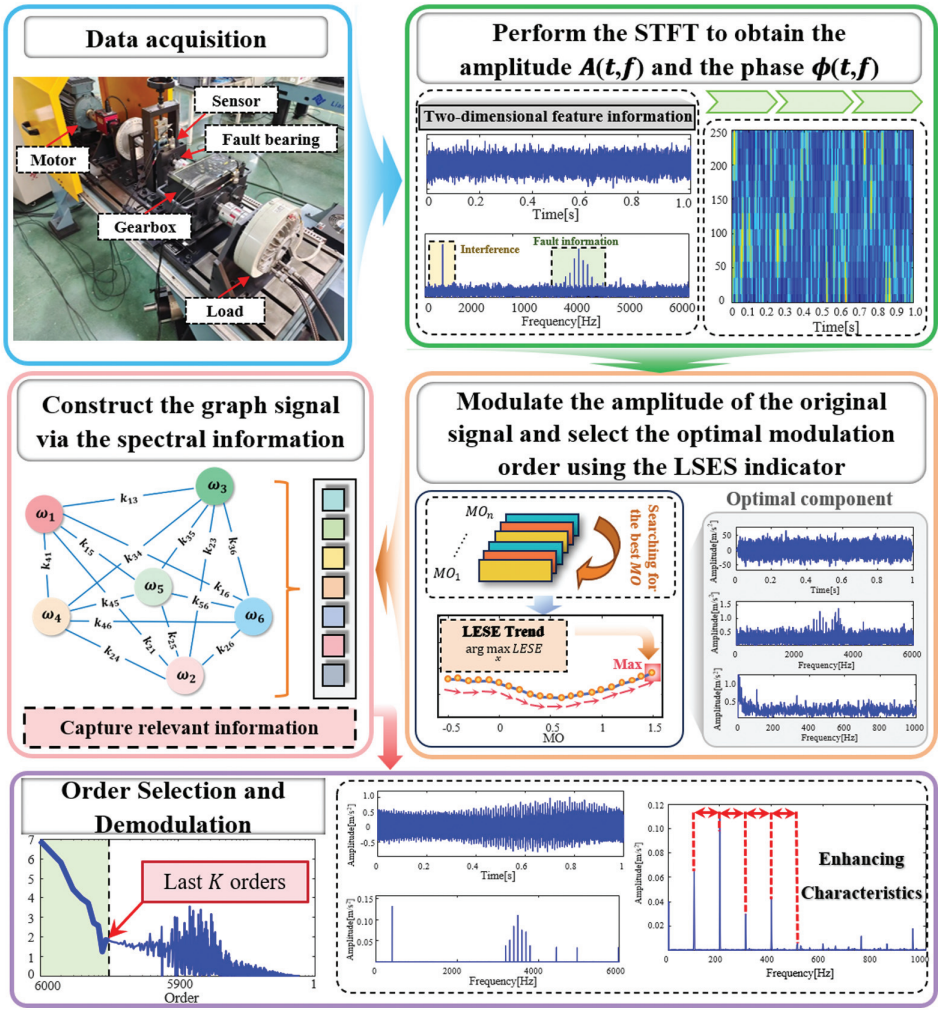

Fig. 1. Flowchart of the proposed amplitude-modulated graph spectrum method.

process cumbersome but also easily introduces subjective errors, increases the risk of misdiagnosis, and makes it difficult to achieve adaptive and reliable extraction of fault characteristics.

Therefore, it is necessary to develop an evaluation indicator that can effectively characterize the energy level of fault-induced impulse components in the corrected signal. To this end, this paper proposes a new evaluation metric, namely the LSES, for adaptive selection of the optimal MO parameters.

In 1990, Hosking first proposed the concept of linear moments (L-moments) based on the theory of order statistics and systematically explained its mathematical properties and calculation methods. Suppose a sequence of random variables has $i-th$ order linear moments. The samples are sorted in this sequence in ascending order of their numerical values. The corresponding order statistics can be obtained $X_{1:i} \le X_{2:i} \le \cdots \le X_{i:i}$. Then the linear moments of X can be expressed as:

$$\lambda_i = \frac{1}{r} \cdot \sum_{k=0}^{i-1} (-1)^k \cdot C_k^{i-1} \cdot E(X_{i-k:i}), \quad i = 1,2\ldots \tag{3}$$

where C_k^{i-1} represents the number of combinations corresponding to selecting k from $i-1$ random variables, $X_{(i-k:i)}$ is the smallest order statistic, and $E(\cdot)$ represents the expected value of the random sample.

When the sample size of a random sample sequence is n, the expected value of its i-th order statistic can be expressed as:

$$E(X_{i:n}) = \frac{n_!}{(i-1)! \cdot (n-i)!} \cdot \int_0^1 x(F) \cdot [F(x)^{i-1}] \cdot g[1-F(x)]^{n-i} dF(x) \tag{4}$$

The first four linear moments are calculated using the above formula:

$$\begin{aligned}
\lambda_1 &= E(X_{1:1}) = b_0 \\
\lambda_2 &= \frac{1}{2} E(X_{2:2} - X_{1:2}) = 2b_1 - b_0 \\
\lambda_3 &= \frac{1}{3} E(X_{3:3} - 2X_{2:3} + X_{1:3}) \\
&= 6b_2 - 6b_1 + b_0 \\
\lambda_4 &= \frac{1}{4} E(X_{4:4} - 3X_{3:4} + 3X_{2:4} - X_{1:4}) \\
&= 20b_3 - 30b_2 + 12b_1 - b_0
\end{aligned} \tag{5}$$

where $b_i = \int_0^1 x(F) \cdot [F(x)]^i dF(x)$, $i = 0,1,2,3$ is the $i-th$ order weight probability moment. However, for a real discrete signal, the probability distribution function is

often difficult to obtain, making it hard to derive the linear moments from the probability distribution function. Therefore, we use an unbiased estimate of the weighted probability moments instead of calculation, as defined below:

$$\widehat{b}_i = \frac{1}{n}\sum_{k=i+1}^{n}\frac{(k-1)(k-2)\ \cdots\ (k-i)}{(n-1)(n-2)\ \cdots\ (n-i)}x_{(k)} \tag{6}$$

Hosking's definition of linear kurtosis is given as:

$$LK = \frac{\lambda_4}{\lambda_2} \tag{7}$$

Then, for any discrete random sequence, the estimated value of LK is

$$LK = \frac{\widehat{\lambda}_4}{\widehat{\lambda}_2} \tag{8}$$

Let $ES(f)$ represent the envelope spectrum. Performing a Fourier transform on it yields its spectrum as follows:

$$SES = |FT[ES(f)]| \tag{9}$$

To reduce the impact of sporadic pulses and external harmonic interference on the analysis results, the components of the envelope signal near the origin of the spectrum are set to zero. Based on this, the defined envelope spectrum kurtosis can be further expressed as:

$$LSES = \frac{\lambda_4(SES)}{\lambda_2(SES)} \tag{10}$$

b) Amplitude modulation spectrum model construction method

Graph theory, as an effective framework for analyzing graph-structured data, has been widely applied in machine learning, dimensionality reduction, and intelligent information processing, with its core lying in extracting structural information from graph matrices through spectral analysis based on eigenvalues and eigenvectors to characterize graph properties. The GFT serves as a fundamental technique that converts graph signals from the vertex domain into the graph spectral domain, enabling the representation of intrinsic signal patterns in the frequency domain. However, in practical applications, periodic impulse components in time-domain signals are often severely masked by noise interference, which makes fault feature extraction increasingly difficult. Therefore, this paper employs the GFT to aggregate fault-related information in the frequency domain, thereby achieving more effective extraction of fault features.

The previous section identified the optimal correction signal through index screening. However, noise interference still exists in its time-domain waveform, making fault diagnosis difficult. To address this issue, we combine spectral graph theory with the amplitude information of the optimal correction signal to construct a graph signal and perform fault diagnosis.

First, the selected corrected signal is transformed into the frequency domain using the fast Fourier transform (FFT), from which the amplitude and phase spectra are derived. The amplitude data are given by:

$$Re(f) = |S_m(f)| \tag{11}$$

where $S_m(f)$ denotes the frequency-domain representation of the selected corrected signal.

A graph signal is constructed using amplitude information, and a GFT is performed on the graph signal to obtain the frequency-domain spectrum, and then the frequency-domain spectrum model is defined as follows:

$$\widehat{g}(f) = \sum_{n=0}^{N-1} Re(n)\cdot l_f(n),\ f = 0,1,2\ldots,N-1 \tag{12}$$

where $\widehat{g}(f)$ indicates the spectral sequence in the frequency domain and l_f denotes the associated eigenvector. The selected spectral order in $\widehat{g}'(f)$ is then reconstructed through the inverse GFT, which is formulated as follows:

$$Re'(q) = \sum_{f=0}^{N-1} l_p(q)\cdot \widehat{g}'(f),\ q = 0,1,2\ldots,N-1 \tag{13}$$

Figure 2(a) shows the reconstruction order of the spectrum, with the horizontal axis range corresponding to the frequency. (b-d) shows the time-domain waveforms

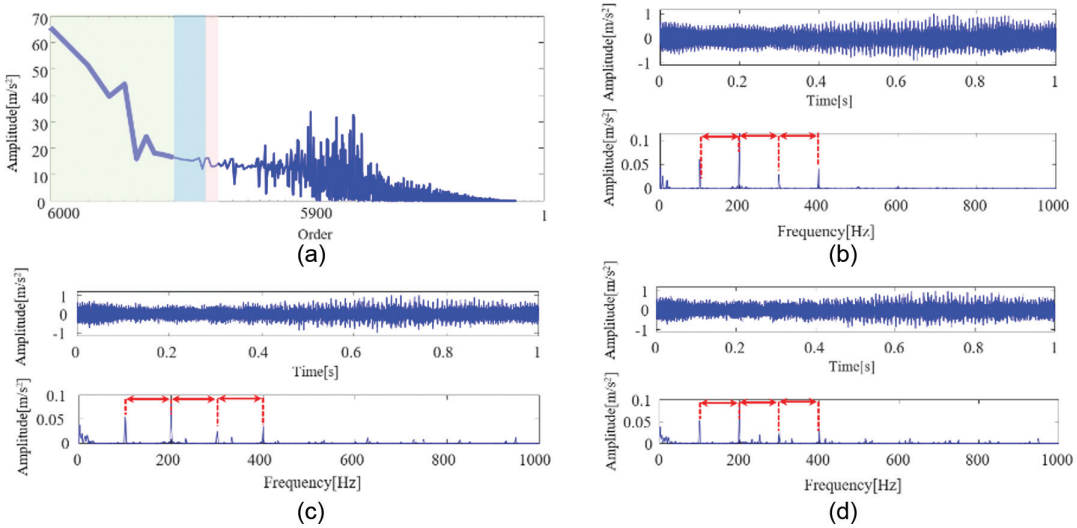

Fig. 2. Graph reconstruction order and the reconstructed time-domain signal and envelope spectrum.

and envelope spectra after reconstruction at different orders. (b) illustrates the reconstruction results for the last 10 orders, (c) illustrates the reconstruction results for the last 20 orders, and (d) illustrates those for the last 25 orders.

As shown in Fig. 2 (b–d), the processing effects obtained by selecting different reconstruction orders are not significantly different. Therefore, in subsequent simulations and experimental processing, we should select as few reconstruction orders as possible while ensuring significant processing effects to improve computational efficiency.

III. SIMULATION VERIFICATION

Bearing vibration signals usually contain a large amount of noise, which significantly interferes with the accurate extraction of fault features and the identification of fault conditions. To address this issue, this paper proposes an amplitude modulation graph model, which can effectively suppress part of the noise components in the original bearing vibration signal while enhancing fault-related feature information, thereby improving the accuracy of fault diagnosis. In this section, a set of simulated signals is constructed to verify the effectiveness of the proposed method.

Among them, the random impact component is used to simulate stochastic transient disturbances generated during equipment operation; the modulated signal interference is used to represent amplitude modulation effects caused by multi-source coupling under complex operating conditions; the bearing outer race fault signal is used to characterize the periodic impact response induced by local damage on the outer race of the bearing; and the random noise is used to simulate background noise interference in real acquisition environments. By constructing the above multi-component mixed simulated signal, the vibration characteristics of bearings under complex operating conditions can be more realistically represented, providing a reliable basis for verifying the noise reduction and feature enhancement capability of the proposed method. The simulated signal is constructed as follows:

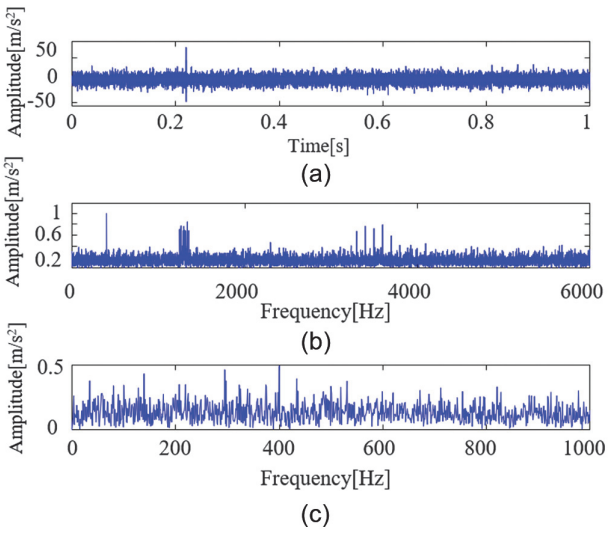

Fig. 3. Simulated signal: (a) time-domain waveform, (b) frequency spectrum, and (c) envelope spectrum.

$$\begin{cases} s_1(t) = \sum_{k=1}^{K} A_1 e^{-g_i \cdot 2\pi f_{n1}(t-kT_1)} \cdot \sin(\sqrt{1-g_1^2} \times 2\pi f_{n1}(t-kT_1))u(t-kT_1) \\ s_2(t) = A_2 \sin(2\pi f_1 t) \sin(2\pi f_2 t + \sin(2\pi f_3 t)) \\ s_3(t) = A_3 e^{-g_2 \cdot 2\pi f_{n2}(t-kT_2)} \cdot \sin(\sqrt{1-g_2^2} \times 2\pi f_{n2}(t-kT_2))u(t-kT_2) \\ s_4(t) = \sin(2\pi f_4 t) \\ s(t) = s_1(t) + s_2(t) + s_3(t) + s_4(t) + n(t) \end{cases} \tag{14}$$

where in $s_1(t)$ is the repetitive impact signal generated by the simulated bearing outer ring fault, with amplitude $A_1 = 5$, system natural frequency $f_{n1} = 3500$ Hz, damping coefficient $g_1 = 0.038$, and impact period $T = 0.01s$. The fault characteristic frequency is $f_o = 100$Hz. $u(t)$ is the unit step function, and the number of impacts is $K = [N/(F_s T)] + 1$. This parameter setting ensures that adjacent impacts do not overlap, thus conforming to the vibration characteristics of a typical bearing outer ring fault. $s_2(t)$ is used to simulate non-stationary modulation interference signals caused by factors such as gear meshing, rotor misalignment, or eccentricity during equipment operation, where the amplitude is $A_2 = 4$, the amplitude modulation frequency is $f_1 = 20$ Hz, the carrier frequency is $f_2 = 1300$ Hz, and the frequency modulation frequency is $f_3 = 33$ Hz. s_3 represents an accidental impact, with amplitude $A_2 = 4$, natural frequency $f_{n2} = 2000$ Hz, damping coefficient $g_2 = 0.1$, and impact period $T = 0.00625$ s. s_4 represents harmonic interference, $f_4 = 400$ Hz. The amplitude of Gaussian white noise $n(t)$ is set to -10 dB, the sampling frequency is $F_s = 12000$ Hz, and the signal length is set to $N = 12000$ sampling points. Figure 3 presents the simulated signal in the time, frequency, and envelope spectrum domains.

As shown in the figure, under the joint influence of multiple disturbances, the fault-related frequency components in the envelope spectrum are severely masked by noise and modulation effects, which makes the fault information difficult to extract and poses a considerable challenge to fault diagnosis.

Subsequently, the proposed amplitude modulation spectrum model processed the constructed simulation signal to verify its capability to extract fault feature information under complex interference conditions.

First, the proposed method performs time–frequency amplitude modulation on the original signal. This process highlights the effective feature components in the signal by modulating the amplitude information in the time and frequency domains, while suppressing background noise and irrelevant interference components to a certain extent, thereby achieving preliminary noise reduction of the original signal. After amplitude modulation, different MOs lead to distinct effects on fault feature amplification and noise attenuation. Therefore, it is necessary to further determine the optimal MO to obtain the best signal processing effect. By introducing the LSES indicator, the method calculates the LSES value of the signal corresponding to each MO, quantitatively analyzes the different modulation results, and

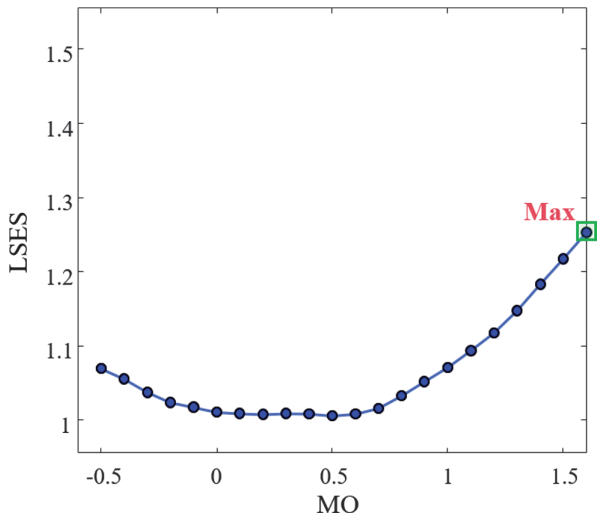

Fig. 4. Selection of the optimal modulation order based on the LSES indicator.

selects the MO corresponding to the optimal LSES value as the optimal modulation parameter. The selection results of LSES are shown in Fig. 4. Finally, the modulated signal corresponding to the optimal MO is selected as the input for subsequent processing, enabling further fault feature extraction and fault diagnosis.

The GFT maps the optimal modulated signal into the graph spectral domain, thereby deriving its graph frequency representation. The GFT maps the modulated signal into the graph frequency domain, thereby enabling a more effective characterization of the signal's frequency features within the graph structure. After obtaining the graph spectral representation, an appropriate spectral order is selected according to the fault characteristic distribution. The selected spectral components are retained, and the inverse GFT maps the filtered graph spectrum information back to the temporal domain to reconstruct the signal. This process preserves fault-related features while suppressing irrelevant interference components, thereby improving the time-domain representation of fault information. Subsequently, the reconstructed time-domain signal is analyzed using the Fourier transform to obtain its spectral characteristics. Meanwhile, the Hilbert transform is employed to extract the signal envelope and derive the envelope spectrum, thereby highlighting the characteristic frequency components associated with fault impacts. Figure 5 presents the selection of the graph spectral reconstruction order, as well as the reconstructed time-domain waveform and its corresponding envelope spectrum.

The reconstructed waveform and the corresponding envelope spectrum reveal a marked improvement in fault feature representation. The reconstructed waveform shows more pronounced repetitive impacts, indicating that fault-sensitive components are successfully extracted from the interference-dominated signal. The envelope spectrum further reveals the dominant fault frequency and its harmonic structure, thereby supporting accurate bearing fault identification. In particular, not only the fundamental fault characteristic frequency can be identified in the envelope spectrum, but also its higher-order harmonic components are observed, with the highest reaching up to eight times the fault characteristic frequency. This further validates the effectiveness of the proposed method in enhancing and extracting fault features.

IV. EXPERIMENTAL VERIFICATION OF OUTER RACE FAULT

The outer race fault experimental data used in this section are derived from the outer race crack test signal provided by the Wuxi Houde bearing experimental platform. The tested bearing is a deep groove ball bearing of type SKF6205, which can effectively simulate the vibration response characteristics of a bearing with a localized outer race crack under actual engineering conditions. The experimental signal is sampled at 16 kHz with an SNR of −15 dB to evaluate the fault feature extraction performance under severe noise contamination. Based on the bearing geometry and rotational speed, the characteristic frequency associated with the outer race defect is determined as 179 Hz. The signal provides a challenging case for assessing the fault feature extraction capability of the proposed method under severe background interference. Figure 6 shows the original signal. The signal is subsequently analyzed using the proposed method, with the resulting outputs illustrated in Fig. 7.

The envelope spectrum of the original signal shows that severe noise contamination obscures the defect-related frequency and its harmonics. Consequently, the fault-related feature information cannot be effectively separated

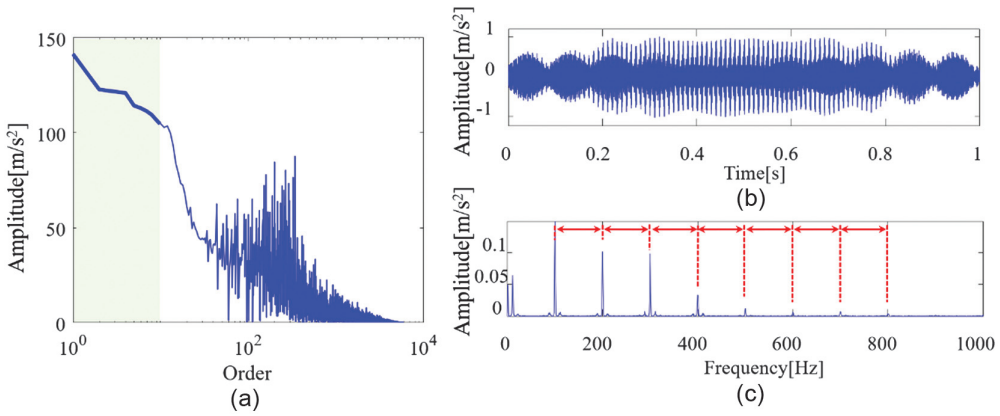

Fig. 5. (a) Selection of the graph spectral reconstruction order; (b) reconstructed time-domain signal; and (c) envelope spectrum of the reconstructed signal.

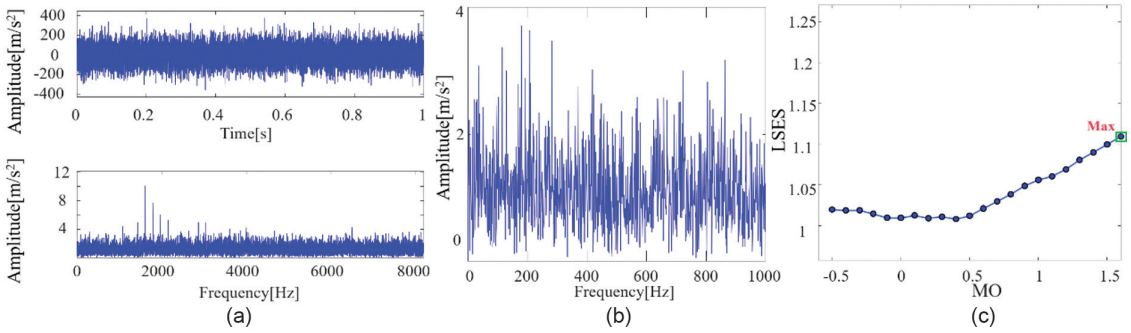

Fig. 6. (a) Time-domain signal and spectrum of the bearing outer race fault; (b) envelope spectrum of the bearing outer race signal; and (c) optimal order selection based on the indicator.

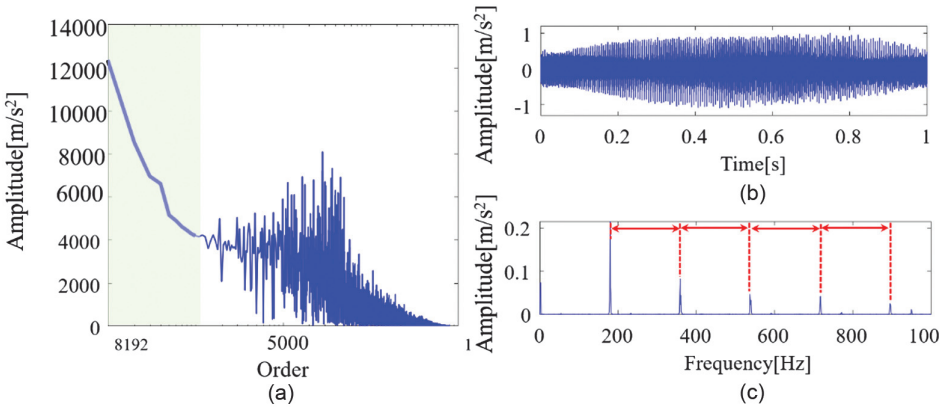

Fig. 7. Bearing outer race fault: (a) graph spectral reconstruction order; (b) reconstructed time-domain signal; and (c) envelope spectrum of the reconstructed signal.

or identified, resulting in ambiguous diagnostic outcomes and increased difficulty.

The processed waveform and its envelope spectrum display prominent fault-related signatures. The reconstructed waveform presents clearly periodic impact responses, demonstrating the effective enhancement of fault-sensitive components. Meanwhile, the envelope spectrum of the reconstructed signal is considerably cleaner, with noise interference significantly suppressed. The defect-related frequency and its harmonic structure are readily observable, further validating the proposed method in strengthening fault signatures and reducing noise interference.

V. EXPERIMENTAL VERIFICATION OF INNER RACE FAULT

An additional dataset from the Wuxi Houde bearing test platform is used to evaluate the proposed method's ability to identify inner race defect signatures. The selected data correspond to an inner race crack fault signal with an SNR of −12 dB, and the characteristic frequency of the inner race fault is $f_i = 270$ Hz. Figure 8 displays the original signal, while Fig. 9 illustrates the corresponding outputs generated by the proposed method.

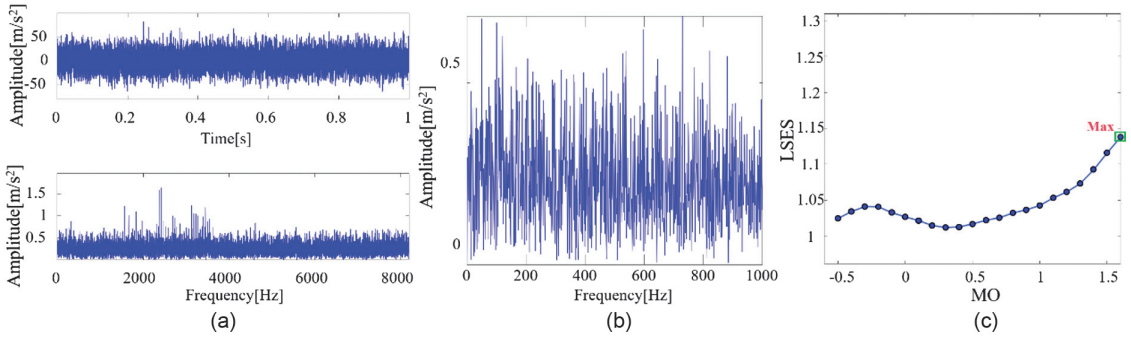

Fig. 8. (a) Time-domain signal and spectrum of the bearing inner race fault; (b) envelope spectrum of the bearing inner race signal; and (c) optimal order selection based on the indicator.

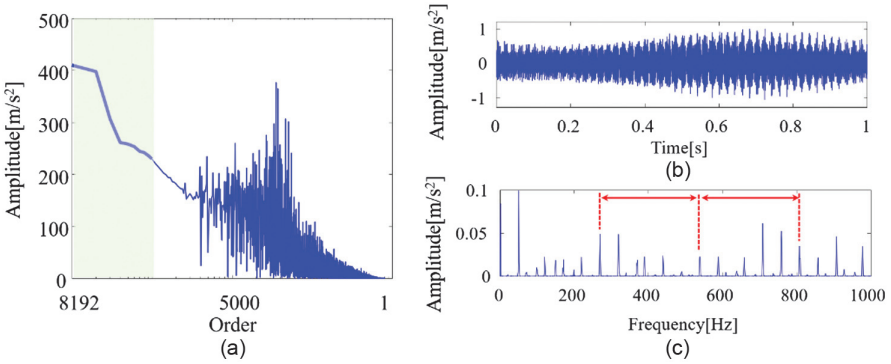

Fig. 9. Bearing inner race fault: (a) selection of the graph spectral reconstruction order; (b) reconstructed time-domain signal; and (c) envelope spectrum of the reconstructed signal.

For the original inner race defect signal, the envelope spectrum shows that the defect-related frequency and its harmonic structure are heavily buried by strong background noise, and the frequency component associated with the inner race defect, together with its harmonic structure, is heavily obscured, resulting in weak fault-sensitive representation. As a result, the fault features in the envelope spectrum are not sufficiently prominent, which brings considerable difficulty to the accurate identification of the inner race fault.

From the processed time-domain signal and envelope spectrum, the presence of fault information can be clearly identified. In the time-domain waveform, the fault-induced impulses exhibit a pronounced periodic pattern, indicating stable and repetitive impact behavior associated with the inner race defect. The envelope spectrum clearly identifies the primary defect frequency together with its second and third harmonics, which further verifies the proposed method's ability to strengthen weak fault signatures in noise-contaminated environments.

This section presents experimental validations for both bearing outer race and inner race faults using typical fault data obtained from the Wuxi Houde bearing experimental platform. A severe noise-contaminated case is used to assess the robustness of the proposed method. The obtained results indicate that the method reduces random noise and non-stationary disturbances, while making fault-induced impact signatures more prominent. Consequently, the envelope spectrum presents a clearer defect-frequency component and harmonic structure.

Moreover, consistent results are obtained for both outer race and inner race fault cases, indicating that the proposed method can stably extract key fault information. This further verifies its strong capability in fault feature enhancement and its applicability under complex operating conditions, providing a reliable basis for bearing fault diagnosis in practical engineering applications.

VI. CONCLUSIONS

This paper addresses the difficulty of effective fault feature extraction of bearings under strong noise environments by proposing a bearing fault diagnosis method based on an amplitude modulation spectrum graph. The method first constructs an amplitude modulation processing framework based on the STFT and introduces the LSES index to achieve adaptive optimization of the MO, thereby obtaining the optimal modulated signal. On this basis, a graph signal model is constructed, and the signal is mapped into the graph spectrum domain via GFT. High-order spectral components are then selected for inverse transformation, enabling the synergistic enhancement of fault features and suppression of noise.

The simulation results, together with experimental validations on bearing outer race and inner race fault signals, demonstrate that the proposed method can effectively highlight periodic impact characteristics under strong noise conditions. The defect-frequency component and its harmonic structure are markedly strengthened, thereby improving the identification of weak fault signatures. Compared with conventional signal processing methods, the proposed approach exhibits stronger robustness and adaptability in weak fault feature extraction.

In summary, the proposed method can effectively improve the observability and separability of bearing fault features under complex operating conditions, providing an effective signal analysis approach for bearing condition monitoring and fault diagnosis. It demonstrates certain potential for engineering applications.

ACKNOWLEDGMENTS

The authors sincerely acknowledge the support of the Young Scientists Fund of the National Natural Science Foundation of China (Grant No. 52405083).

CONFLICT OF INTEREST STATEMENT

The authors declare that they have no conflicts of interest related to this work.

REFERENCES

[1] Y. Zhang *et al.*, "A dual-component elastic adaptation network for rotating machinery incremental fault diagnosis under variable operating conditions," *J. Dyn. Monit. Diagn.*, vol. 5, pp. 49–63, 2026.

[2] C. Ma *et al.*, "Feature identification based on cepstrum-assisted frequency slice function for bearing fault diagnosis," *Measurement*, vol. 246, p. 116753, 2025.

[3] M. Spirto *et al.*, "A comparative study between SDP-CNN and time-frequency-CNN-based approaches for fault detection," *J. Dyn. Monit. Diagn.*, vol. 5, pp. 25–37, 2026.

[4] Z. Shao *et al.*, "PLL-WCAN: Pseudo-label progressive learning guided wavelet class-aware adaptive network for gearbox cross-domain fault diagnosis," *Mech. Syst. Signal Process.*, vol. 230, p. 112624, 2025.

[5] L. Ge *et al.*, "High-dimensional optimized extraction chirplet transform: Algorithm and applications," *ISA Trans.*, vol. 169, pp. 520–534, 2026.

[6] J. Li, W. Luo, and M. Bai, "Review of research on signal decomposition and fault diagnosis of rolling bearing based on vibration signal," *Meas. Sci. Technol.*, vol. 35, no. 9, p. 092001, 2024.

[7] Z. Ge, "Review on data-driven modeling and monitoring for plant-wide industrial processes," *Chemom. Intell. Lab. Syst.*, vol. 171, pp. 16–25, 2017.

[8] S. Yin *et al.*, "A review on recent development of spacecraft attitude fault tolerant control system," *IEEE Trans. Ind. Electron.*, vol. 63, no. 5, pp. 3311–3320, 2016.

[9] Y. Huangfu *et al.*, "Meshing and dynamic characteristics analysis of spalled gear systems: A theoretical and experimental study," *Mech. Syst. Signal Process.*, vol. 139, p. 106640, 2020.

[10] C. Ma *et al.*, "A dual-objective optimized reweighted overlapping group sparse framework integrating frequency slice function for robust bearing fault diagnosis," *Mech. Syst. Signal Process.*, vol. 242, p. 113678, 2026.

[11] J. Chen *et al.*, "A convex optimization difference analysis model for intelligent fault detection and diagnosis of gearboxes," *Mech. Syst. Signal Process.*, vol. 251, p. 114207, 2026.

[12] Y. Huangfu *et al.*, "Fault tracing of gear systems: An in-situ measurement-based transfer path analysis method," *J. Sound Vib.*, vol. 553, p. 117610, 2023.

[13] H. Jo *et al.*, "An upper-probability-based softmax ensemble model for multi-sensor bearing fault diagnosis," *Sensors*, vol. 25, p. 6887, 2025.

[14] Z. Jiang, D. Liu, and L. Cui, "A temporal-spatial multi-order weighted graph convolution network with refined feature topology graph for imbalance fault diagnosis of rotating machinery," *Reliab. Eng. Syst. Saf.*, vol. 257, p. 110830, 2025.

[15] A. Moshrefzadeh, A. Fasana, and J. Antoni, "The spectral amplitude modulation: A nonlinear filtering process for diagnosis of rolling element bearings," *Mech. Syst. Signal Process.*, vol. 132, pp. 253–276, 2019.

[16] Z. Sheng, K. Zhang, and Q. Liao, "Equalization filtering technology based on differential spectral amplitude modulation and its application in bearing fault diagnosis," *Meas. Sci. Technol.*, vol. 37, no. 13, p. 136101, 2026.

[17] K. Zhang *et al.*, "Variational filtering differential strategy with amplitude modulation for fault feature extraction," *Meas. Sci. Technol.*, vol. 37, no. 10, p. 106105, 2026.

[18] W. Xie *et al.*, "Graph-based multimodal semi-supervised image classification," *Neurocomputing*, vol. 138, pp. 167–179, 2014.

[19] F. R. Chung, *Spectral Graph Theory*. Providence, RI, USA: American Mathematical Society, 1997.

[20] A. Sandryhaila and J. M. F. Moura, "Discrete signal processing on graphs," *IEEE Trans. Signal Process.*, vol. 61, no. 7, pp. 1644–1656, 2013.